





TIME SERIES OF SURFACE WATER DISSOLVED INORGANIC CARBON ISOTOPES FROM THE SOUTHERN CALIFORNIA BIGHT

Niels E Hauksson^{1*}  • Xiaomei Xu¹  • Shawn Pedron^{1,2}  • Hector A Martinez¹ • Christian B Lewis^{1,3} • Danielle S Glynn⁴ • Christopher Glynn⁵ • Noreen Garcia⁶ • Alessandra Flaherty⁷ • Katherine Thomas¹ • Sheila Griffin¹ • Ellen R M Druffel¹ 

¹Earth System Science Dept., University of California, Irvine, CA 92617, USA

²Lawrence Livermore National Laboratory, 7000 East Avenue, Livermore, CA 94550, USA

³National Isotope Centre, GNS Science, Lower Hutt, New Zealand

⁴Ocean Sciences Dept., University of California, Santa Cruz, CA 95064, USA

⁵Northrup Grumman, Utah, USA

⁶Marine Chemistry and Geochemistry, Scripps Institution of Oceanography, U.C. San Diego, La Jolla, CA, USA

⁷Division of Geological and Planetary Sciences, California Institute of Technology, Pasadena, CA, USA

ABSTRACT. Dissolved inorganic carbon (DIC) in ocean water is a major sink of fossil fuel derived CO₂. Carbon isotopes in DIC serve as tracers for oceanic water masses, biogeochemical processes, and air-sea gas exchange. We present a timeseries of surface DIC δ¹³C and Δ¹⁴C values from 2011 to 2022 from Newport Beach, California. This is a continuation of previous timeseries (Hinger et al. 2010; Santos et al. 2011) that together provide an 18-year record. These data show that DIC Δ¹⁴C values have declined by 42‰ and that DIC δ¹³C values have declined by 0.4‰ since 2004. By 2020, DIC Δ¹⁴C values were within analytical error of nearby clean atmospheric CO₂ Δ¹⁴C values. These long-term trends are likely the result of significant fossil fuel derived CO₂ in surface DIC from air-sea gas exchange. Seasonally, Δ¹⁴C values varied by 3.4‰ between 2011 and 2022, where seasonal δ¹³C values varied by 0.7‰. The seasonal variation in Δ¹⁴C values is likely driven by variations in upwelling, surface eddies, and mixed layer depth. The variation in δ¹³C values appears to be driven by isotopic fractionation from marine primary producers. The DIC δ¹³C and Δ¹⁴C values record the influence of the drought that began in 2012, and a major upwelling event in 2016.

KEYWORDS: coastal, environment, radiocarbon, stable isotopes, water.

1. INTRODUCTION

Marine dissolved inorganic carbon (DIC) is the largest exchangeable reservoir of carbon in the surface ocean, and it exchanges with atmospheric CO₂ on annual to decadal timescales (Broecker and Peng 1982). As humans have released additional CO₂ into the atmosphere, DIC has acted as a major sink for some of this additional carbon (Sabine et al. 2004; Gruber et al. 2019). This increase in DIC lowers the ocean's pH, which has profound impacts on ocean ecosystems (Feely et al. 2004). A key tool used to track DIC are its carbon isotopes (¹³C and ¹⁴C), as they are reflective of the circulation and biogeochemistry of the water mass in which DIC is dissolved. These isotopes also reflect the anthropogenic impact on the global carbon cycle. First, above-ground thermonuclear bomb testing nearly doubled the ¹⁴C content of atmospheric CO₂ by the early 1960s. Due to the relatively long isotopic equilibration time of CO₂, this resulted in a smaller, but longer-lived increase in surface marine DIC Δ¹⁴C (Druffel 1989). Second, the burning of fossil fuels since 1890 released CO₂ with no ¹⁴C and less ¹³C than atmospheric CO₂ that has reduced the overall isotopic ratios, contributing to the Suess effect (Suess 1953). The decrease in ¹⁴C/¹²C and ¹³C/¹²C ratios have also been observed in marine DIC (Andrews et al. 2016; Brooks 2020). Thus, attempts by the international community to curb CO₂ emissions will likely be reflected in future DIC isotopic records.

*Corresponding author. Email: nhaukss@uci.edu

The $^{13}\text{C}/^{12}\text{C}$ ratio of DIC is the result of equilibrium isotope effect and kinetic isotope effect acting on the sources and sinks of DIC. For example, the $^{13}\text{C}/^{12}\text{C}$ of surface DIC ($\delta^{13}\text{C} \approx 1\text{‰}$) is higher than that of atmospheric CO_2 ($\delta^{13}\text{C} \approx -8\text{‰}$), because equilibrium processes favor a higher proportion of the heavier isotope in the more condensed phase (Mook 1986). A non-equilibrium process, like biological uptake, favors the lighter isotope due to its higher diffusivity. Marine phytoplankton are thus, depleted in ^{13}C ($\delta^{13}\text{C} \approx -21\text{‰}$) relative to surface DIC (Mook 1986). In regions with significant phytoplankton growth, this can also measurably raise the $^{13}\text{C}/^{12}\text{C}$ ratio of the remaining DIC (Kroopnik 1985). Conversely, remineralization of sinking marine phytoplankton by zooplankton and microbes releases ^{13}C -depleted DIC, which then lowers the overall $^{13}\text{C}/^{12}\text{C}$ of the subsurface DIC (Kroopnik 1985).

While ^{14}C also undergoes isotopic fractionation, reported $^{14}\text{C}/^{12}\text{C}$ ratios are corrected for any fractionation (Stuiver and Polach 1977). Therefore, the primary control on a measured $^{14}\text{C}/^{12}\text{C}$ ratio is the radioactive decay of ^{14}C and the mixing of carbon pools with different $^{14}\text{C}/^{12}\text{C}$ ratios. In the surface ocean, newly dissolved CO_2 mixes with DIC from the surface water. In the pre-bomb era, this resulted in surface DIC with $^{14}\text{C}/^{12}\text{C}$ ratios ($\Delta^{14}\text{C} \approx -60$) lower than that of atmospheric CO_2 ($\Delta^{14}\text{C} \approx 0$) (Stuiver et al. 1986). The equilibration time of ^{14}C by air-sea exchange of CO_2 is about 10 years, which is far longer than the mixing time of surface waters (Broecker and Peng 1982). Thus, shifts in the $^{14}\text{C}/^{12}\text{C}$ ratio in surface DIC during this period are almost entirely due to mixing of surface and upwelled waters within a region. The introduction of bomb radiocarbon to the atmosphere produced a large isotopic gradient with the ocean that increased the $\Delta^{14}\text{C}$ of surface DIC by $\sim 200\text{‰}$ (Druffel et al. 2016). As the $^{14}\text{C}/^{12}\text{C}$ of atmospheric CO_2 has declined due to redistribution of bomb-derived ^{14}C and the ^{14}C -free CO_2 from fossil fuels, the surface DIC $^{14}\text{C}/^{12}\text{C}$ ratios have also declined, albeit at a slower rate (Hinger et al. 2010; Santos et al. 2011; Andrews et al. 2016). In the last few years, atmospheric CO_2 reached its pre-bomb $^{14}\text{C}/^{12}\text{C}$ ratio ($\Delta^{14}\text{C} \approx 0\text{‰}$) (Graven et al. 2022). How this ratio and the resulting change in surface DIC carbon isotope ratios will change in the coming years will require continuous monitoring of these carbon pools.

One such monitoring site is located at Newport Beach, California in the Southern California Bight (SCB). The SCB is home to productive marine ecosystems and is characterized by complex circulation of local currents. The northern end of the SCB is at Point Conception ($\sim 34.4^\circ\text{N}$), where the North American coastline turns almost 90° westward and then begins curving southwards (Figure 1). The SCB ends 236 km south of the Mexican-American border, in Baja California ($\sim 32^\circ\text{N}$). The eastern boundary current of the North Pacific Gyre, the California Current, flows southward from Point Conception and dominates the western portion of the SCB (Hickey 1979). This current begins in the subarctic region west of Washington state and is relatively low in temperature and salinity. Closer to the coast, there is the poleward flowing Southern California Countercurrent that brings warmer, nutrient-depleted waters from Baja California. These two currents create a domain scale gyre that can be subdivided into 3 cyclonic eddies (Dong et al. 2009). These eddies can transport warmer, nutrient-poor water east from the North Pacific Gyre to the SCB (Dong et al. 2009). The Southern California Countercurrent dissipates in the spring when wind-driven upwelling creates a westward flow that brings colder, nutrient-rich waters to the surface and stimulates phytoplankton growth (Bray et al. 1999). However, the upwelling in this region is generally weaker than at other points along the Eastern North Pacific (Hickey 1992). The proportions these different water masses present in the SCB at a given time vary based on the prevailing winds (Hickey et al. 2003).



Figure 1 Google Earth image of the Southern California Bight. Arrows show surface currents as described in Hickey (1992). Google, Data LDEO-Columbia, NSF, NOAA, Landsat/Copernicus Data SIO, NOAA, U.S. Navy, NGA, Gebco Data MBARI.

The main subsurface flow in the SCB is the California Undercurrent. This current is formed in the Eastern Equatorial Pacific and is characterized by warm, salty, nutrient-replete, and low-oxygen water (Hickey 1979). Its core generally resides from 200–300 m depth and rises to 100 m during the spring upwelling (Dong et al. 2009; Brogard et al. 2019). CFC-ages between 200–300 m in the SCB indicate that the California Undercurrent’s ventilation age is around 50–125 years (Jeanson et al. 2021; Figure S1). DIC $\Delta^{14}\text{C}$ values from this depth in the SCB have been observed to be 40–90‰ lower than surface DIC values (Figures S2a and S2b) (Key et al. 2015; Olsen et al. 2016). This offset cannot be translated directly into a radiocarbon age due to the presence of bomb radiocarbon. Upwelling results in surface DIC in the SCB with $\Delta^{14}\text{C}$ values that are 50‰ lower than those of surface DIC from the North Pacific Gyre (Figures S3a and S3b) (Key et al. 2015; Olsen et al. 2016). As expected, $\delta^{13}\text{C}$ values of DIC are lower within the California Undercurrent than those in the surface waters of the SCB (Figure S2c) (Key et al. 2015; Olsen et al. 2016). However, the surface DIC $\delta^{13}\text{C}$ values in the SCB are higher than those in the North Pacific Gyre, suggesting that upwelling is not the primary driver of $\delta^{13}\text{C}$ values in the SCB (Figure S3c) (Key et al. 2015; Olsen et al. 2016).

During the past decade, the SCB has had unusually warm temperatures and low rainfall (Frankson et al. 2022). In 2012, the region entered a drought, due to the formation of a persistent ridge of high atmospheric pressure over the Northeast Pacific (Seager et al. 2015). Sea surface temperatures (SST) also abruptly rose due to ocean heat waves between 2013–2015 and 2018–2020 (Bond et al. 2015; Weber et al. 2021). Due to anthropogenic climate change, the

region is expected to continue to warm and to oscillate between extreme dry and extreme wet periods (Berg and Hall 2015). The distinct water masses that contribute to the SCB and the region's sensitivity to climate change make it valuable for understanding both the natural variability of DIC carbon isotopes and the human impact on them.

Hinger et al. (2010) and Santos et al. (2011) reported DIC $\Delta^{14}\text{C}$ and $\delta^{13}\text{C}$ measurements of seawater from the Newport Beach Pier in the Southern California Bight between 2004 and 2010. Here, we present a continuation of this time series that contains mostly monthly records from the Newport Beach Pier between 2011 and 2022. Combined, the nearly two decades of data reflect the natural variability of DIC, the response of DIC to a changing climate, and the effect of fossil fuel CO_2 emissions on the carbon isotopes in DIC.

2. METHODS

2.1 Sample Collection

Sampling was performed monthly at the Newport Beach Pier in Orange County, California (33°36'21"N, 117°55'52"W). Sampling has been conducted since August 2004, with varying gaps in 2009, 2016, 2018, and 2020.

Glass bottles (0.25-L media bottles) were acidified in 10% HCl for 2 hr, rinsed with Milli-Q water, baked at 540°C for 2 hr, and then stored in plastic bags. Sea water was collected via a surface cast of a plastic bucket on a nylon line. The bucket was fitted with a spigot and Teflon tubing that was used to fill the sample bottles. Sample bottles were rinsed three times with sea water and then filled and overflowed for one volume. Samples were poisoned with two drops of saturated mercuric chloride solution and inverted several times after closure. Duplicates were collected for each sampling.

2.2 DIC Extraction

The DIC extraction for ^{14}C samples was performed according to the procedure described by Gao et al. (2014). Briefly, ~45 mL of seawater was subsampled into a 60-mL vial fitted with a Teflon and a Viton septa inside a He-filled glove box. The samples were then acidified with 0.5 mL 85% H_3PO_4 administered using a Hamilton glass syringe with a Sub-Q 26G5/8 gauge needle. The sample vials were then heated on a heatblock at 75°C for 2 hr to convert all DIC to gaseous CO_2 . The CO_2 from the headspace of the sample vial was extracted by a 60-mL syringe with a one-way stopcock. The CO_2 was then loaded onto a vacuum line through a septum for cryogenic purification. Samples were converted to graphite using the sealed tube zinc reduction method over iron catalyst as described by Xu et al. (2007).

The DIC extraction for ^{13}C samples was performed according to a modified procedure described by Torres et al. (2005). One mL of seawater was subsampled into a Labco extainer vial fitted with a Labco septa in a He gas-filled glove box. The samples were then acidified with 50 μL of 85% H_3PO_4 administered with a BD Falcon 1 mL syringe with a 26G5/8 gauge needle. Samples were allowed to equilibrate at room temperature for 12 hr to prevent ^{13}C fractionation of the CO_2 .

2.3 Isotope Analyses

The ^{14}C analyses of the graphite samples were performed at the Keck Carbon Cycle Accelerator Mass Spectrometry (KCCAMS) Laboratory at the University of California, Irvine

(Beverly et al. 2010). Process standards and blanks were performed by dissolving modern coral standard (CSTD), IAEA-C2 and radiocarbon-dead calcite in separate aliquots of previously acidified and stripped sea water using the ^{13}C DIC extraction described above. The results from the calcites were used to correct for sample preparation backgrounds added during DIC extraction and graphitization of samples (Gao et al. 2014). Radiocarbon results are reported as $\Delta^{14}\text{C}$ corrected for collection date (Stuiver and Polach 1977). Uncertainty of $\Delta^{14}\text{C}$ was estimated as $\pm 2.6\text{‰}$ ($\pm 1\sigma$, 31 data points) using the pooled, standard deviation of replicate measurements (McNaught and Wilkinson 1997).

The ^{13}C analysis was performed at UCI using a Gas Bench II coupled with a Thermo Scientific Delta Plus XL isotope ratio mass spectrometer. CO_2 from the sample preparation vials was directly transferred into the Gas Bench via an auto-sampler. DIC concentration was determined with the same IRMS, using a calibration curve derived from calcite standards with various weights. The pooled standard deviation of repeat measurements of $\delta^{13}\text{C}$ was estimated as $\pm 0.05\text{‰}$ ($\pm 1\sigma$, 14 data points). However, due to uncertainties in the $\delta^{13}\text{C}$ values of the standards, we report an uncertainty of 0.1‰ for $\delta^{13}\text{C}$ values. Uncertainty of the concentrations was ± 0.01 mM C based on the pooled standard deviation of repeat measurements ($\pm 1\sigma$, 14 data points).

2.4 Sea Surface Characteristics

Sea surface temperature (SST) and salinity data were obtained from the Scripps Shore Stations program (Carter et al. 2022). Newport Beach lifeguards collected temperatures and water samples daily and sent the samples to Scripps for analysis. The water samples were analyzed for salinity at Scripps Institution of Oceanography (<https://scoos.org/autos>). The Coastal Upwelling Transport Index (CUTI), from NOAA Pacific Fisheries Environmental Laboratory, was used to determine wind-driven upwelling rates at the site (<https://oceanview.pfeg.noaa.gov/products/upwelling>). CUTI uses satellite and in situ wind measurements to estimate the vertical transport of water (Jacox et al. 2018). Our site is very close to the boundary between the 33°N and 34°N CUTI grid boxes. We selected the 33°N box to remain consistent with prior studies (Santos et al. 2011).

3. RESULTS

3.1 DIC Concentration and Isotopes

The DIC $\Delta^{14}\text{C}$, $\delta^{13}\text{C}$ values and DIC concentrations are shown in Table 1 (see Appendix) and Figures 2a–c. The DIC $\Delta^{14}\text{C}$ values ranged from 22.1‰ in March to -12.6‰ in December 2021 (Figure 2a). The DIC $\delta^{13}\text{C}$ values ranged from 2.14‰ in April 2014 to -0.30‰ in October 2015 (Figure 2b). Concentrations varied from 2.04 mM C in October 2020 to 2.68 mM C in August 2013 and the average concentration was 2.29 mM C ($n = 89$) (Figure 2c). The samples collected did not coincide with any major precipitation or runoff events.

3.2 Oceanographic Conditions in the Surface Waters

The 15-day moving average of CUTI ranged from 1.5 m^2/s to -0.2 m^2/s (Figure 2d). Upwelling was typically elevated in the spring and summer months and lower during the winter months. SST ranged from 10.0°C in the winter to 25.2°C in the summer (Figure 2e). Lows in SST during the summers of 2010 and 2017 are likely due to enhanced upwelling or intrusion of the colder

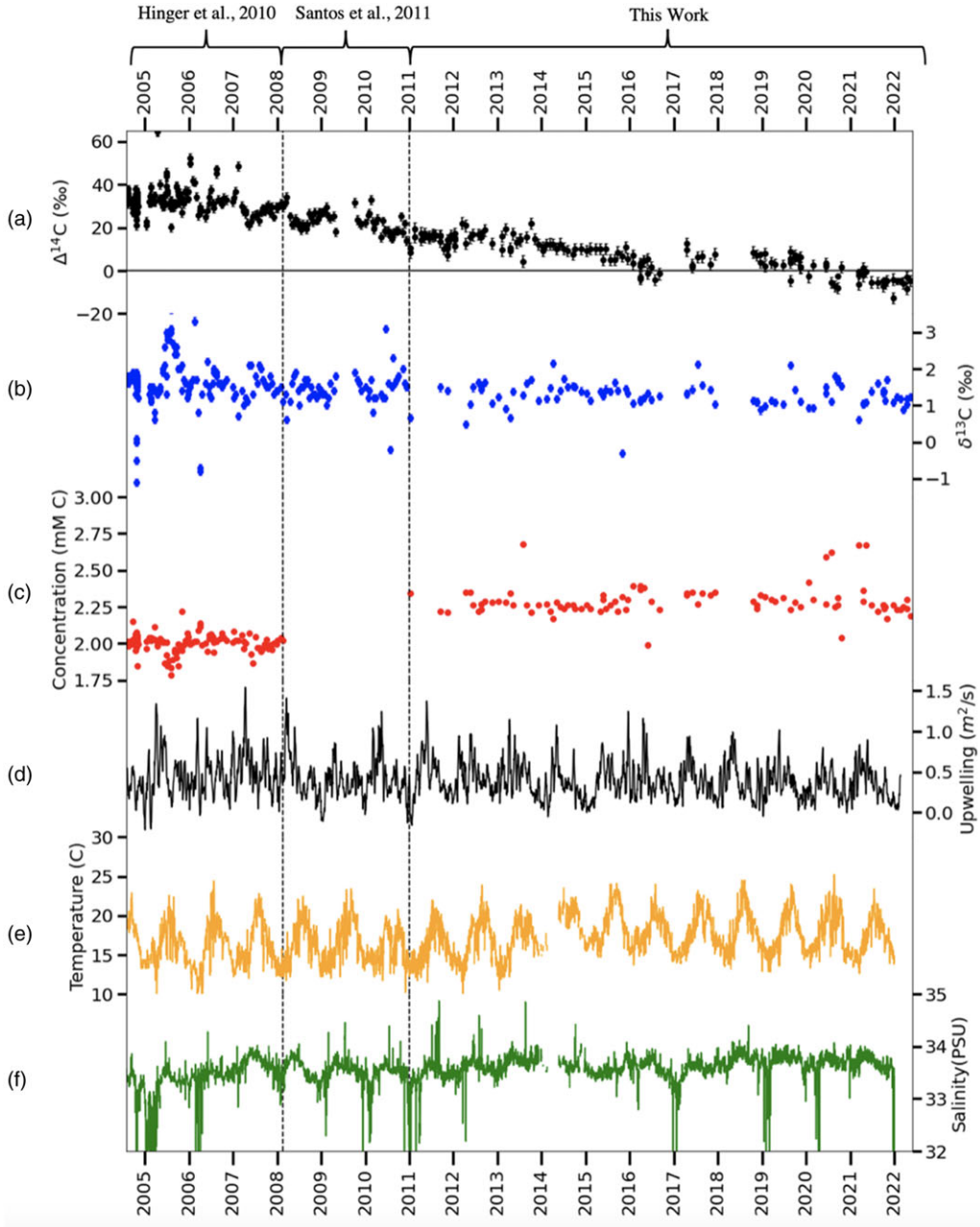


Figure 2 Time series of (a) $\Delta^{14}\text{C}$ values, (b) $\delta^{13}\text{C}$ values, and (c) concentration of surface DIC, (d) the 15-day moving average of CUTI, (e) sea surface temperature, and (f) surface salinity of water samples. Error bars from this work represent the pooled standard deviations of repeated analyses of samples. Error bars for DIC concentration are smaller than the sizes of the symbols. Dashed lines indicate the different sources of data.

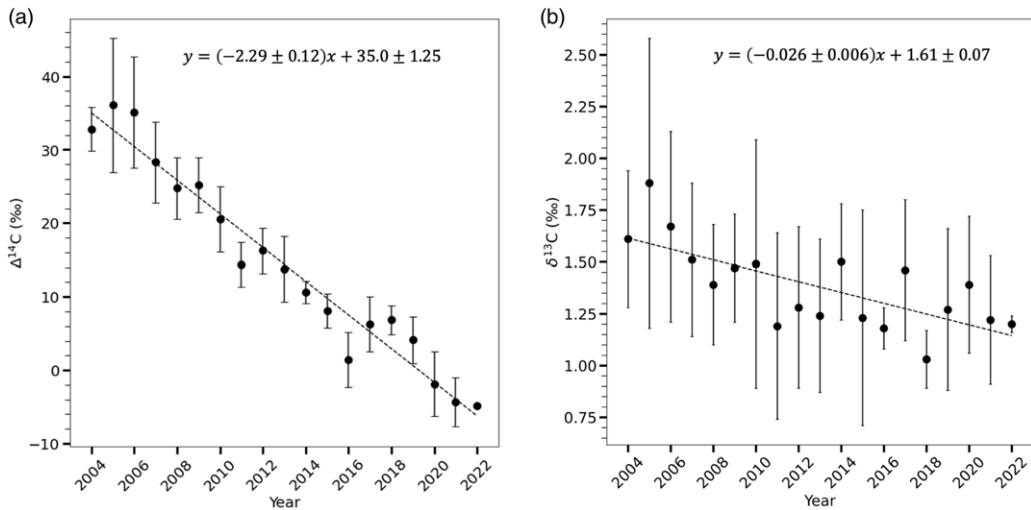


Figure 3 Annual average of (a) $\Delta^{14}\text{C}$ and (b) $\delta^{13}\text{C}$ values of DIC samples from Newport Beach Pier. Dashed lines show model 2 geometric regressions. Error bars represent standard deviation of analyzed samples from that year.

California Current water towards the coast. SST increased markedly in 2014 and remained elevated throughout 2022. Surface salinities ranged from 23.39 practical salinity units (PSU) to 34.87 PSU throughout the 2011–2022 period (Figure 2f). Salinity was lowest and most variable during the winter months and highest during the summer and early fall.

4. DISCUSSION

We present the discussion in three parts. First, we discuss the possible reasons for the decline of the DIC $\Delta^{14}\text{C}$ and $\delta^{13}\text{C}$ values over the past two decades. Second, we discuss the seasonal trends in the DIC $\Delta^{14}\text{C}$ and $\delta^{13}\text{C}$ values and the driving factors behind these trends. Third, we discuss how major climate events between 2011–2022 may have affected the DIC $\Delta^{14}\text{C}$ and $\delta^{13}\text{C}$ values and their trends.

4.1 Decline of DIC $\Delta^{14}\text{C}$ and $\delta^{13}\text{C}$ Values

The long-term trends in $\Delta^{14}\text{C}$ and $\delta^{13}\text{C}$ values were evaluated by performing model 2 geometric regressions of the average annual isotopic values versus the number of years since measurements began in 2004. The regressions were performed using the python package Scipy (Virtanen et al. 2020). These analyses included years with sampling gaps because omission of these years did not change the slope coefficients of the trendlines by more than one standard error.

Annual average DIC $\Delta^{14}\text{C}$ values decreased linearly from 35‰ in 2004 to -6 ‰ in 2022 ($R^2=0.96$, $p<0.001$) (Figure 3a). This is consistent with atmospheric CO_2 observations from La Jolla, California, (32.9°N, 117.3°W), also in the SCB, where atmospheric CO_2 $\Delta^{14}\text{C}$ decreased from 60‰ to -5 ‰ over this same time period (Graven et al. 2022). This indicates that air-sea CO_2 exchange is a significant factor in the long-term trend of surface DIC $\Delta^{14}\text{C}$. Prior to anthropogenic influence, surface DIC $\Delta^{14}\text{C}$ values were lower than those of atmospheric CO_2 due to mixing of surface water with aged water masses and the slow equilibration time

(~10 years) of atmospheric and dissolved $^{14}\text{CO}_2$ (Broecker and Peng 1982). This mixing with aged subsurface waters means that the surface DIC $\Delta^{14}\text{C}$ has a lagged and dampened response to the anthropogenic disturbances in atmospheric CO_2 $\Delta^{14}\text{C}$. In recent years, these two reservoirs have converged. In 2000, annual coral bands in the North Pacific Gyre had $\Delta^{14}\text{C}$ values that were higher than atmospheric CO_2 values (86%) (Andrews et al. 2016), and higher surface water DIC $\Delta^{14}\text{C}$ than maritime air in 2014 from the South China Sea was reported by Gao et al. (2018). Our coastal site has lower DIC $\Delta^{14}\text{C}$ values than surface gyre water due to the local upwelling. As of 2020, DIC $\Delta^{14}\text{C}$ values at Newport Beach pier and atmospheric $^{14}\text{CO}_2$ values are both below 0‰ and within experimental error of one another (Graven et al. 2022). The future relationship of DIC and CO_2 $\Delta^{14}\text{C}$ values at this site is highly dependent on the magnitude of fossil fuel CO_2 emissions in the coming years. Thus, continued monitoring of this site will be invaluable for understanding the magnitude of the ocean carbon sink and the efficacy of our efforts to mitigate climate change.

Annual average DIC $\delta^{13}\text{C}$ values decreased from 1.6‰ in 2004 to 1.2‰ in 2022 ($R^2 = 0.50$, $p = 0.001$) (Figure 3b). This trend is consistent with decreasing $\delta^{13}\text{C}$ of atmospheric CO_2 (Quay et al. 2017) and in the North Pacific Gyre (Brooks 2020). This is likely a further demonstration of the $\delta^{13}\text{C}$ Suess effect as fossil fuel CO_2 emissions continue. It should be noted that the annual variability of $\delta^{13}\text{C}$ (0.7‰) is greater than the total decline observed during this 18-year period (0.4‰). This suggests the possibility that strong seasonality or significant changes in local carbon cycling could mask the Suess effect on DIC $\delta^{13}\text{C}$ in small data sets.

4.2 Seasonality of DIC $\Delta^{14}\text{C}$ and $\delta^{13}\text{C}$

Seasonality was evaluated by comparing the average monthly $\Delta^{14}\text{C}$ and $\delta^{13}\text{C}$ values for the entire data set. As the change in $\Delta^{14}\text{C}$ from 2004–2022 was found to be larger than the annual variation during this time, the $\Delta^{14}\text{C}$ values were detrended assuming a linear trend using Scipy (Virtanen et al. 2020). The annual variation in $\delta^{13}\text{C}$ values was larger than the change in annual averages from 2004 to 2022, so detrending was not performed. Each year was given equal weight when determining monthly averages to account for some years with multiple samples in a single month (Figure 4). Samples on days with salinity <32 PSU were omitted from this analysis. This was done to remove the effect of precipitation events, because changes from these events are highly variable and short-lived (Hinger et al. 2010). These analyses were performed separately for data from Hinger et al. (2010) and Santos et al. (2011) (Figures 3a and 3c) and for the data from this study (Figures 3b and 3d).

Between 2004–2010 (Figure 3a), detrended $\Delta^{14}\text{C}$ values are elevated throughout the winter and early spring, followed by a sharp drop in May and gradual rise in the summer and autumn. Hinger et al. (2010) attributed the elevated $\Delta^{14}\text{C}$ values in the winter to an increase in the number and clustering of small eddies during the winter months. They hypothesized that these eddies transported North Pacific gyre water with higher $\Delta^{14}\text{C}$ values to our site. After 2011, the elevated winter values are not present (Figure 3b). We hypothesize that this could have occurred for two reasons. First, there was less transport of gyre water to our site. During our study period, an atmospheric ridge of persistent high-pressure was formed over the Northeast Pacific (Seager et al. 2015). This ridge drastically reduced the magnitude of the winter winds that possibly could have reduced the eddy strength during this time (Seager et al. 2015). Second, the DIC $\Delta^{14}\text{C}$ values of the Gyre waters have also decreased during this period (Figure S3) (Key et al. 2015; Olsen et al. 2016). As the $\Delta^{14}\text{C}$ values of the surface and upwelled waters converge, this may reduce the strength of the seasonal cycle.

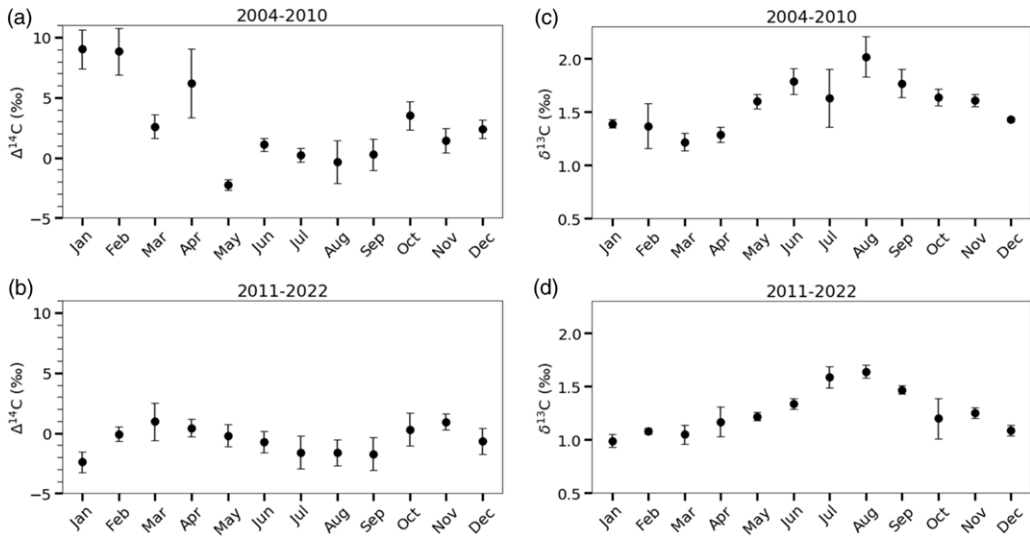


Figure 4 Monthly average of (a) and (b) $\Delta^{14}\text{C}$ and (c) and (d) $\delta^{13}\text{C}$ values of DIC samples from Newport Beach Pier from the (a) and (c) prior timeseries and this work (b) and (d). Error bars represent standard error of the mean for samples available from each month. Samples from 2004–2010 are from Hinger et al. (2010) and Santos et al. (2011). Samples from 2011–2022 are from this work.

The detrended DIC $\Delta^{14}\text{C}$ values from this study period (Figure 3b) display semiannual seasonality with small peaks in March and November and troughs in January and September. The DIC $\Delta^{14}\text{C}$ values vary by 3.4‰ during these cycles, which is less than 2 times the largest standard error in March (2.1‰). The lower DIC $\Delta^{14}\text{C}$ values in winter and summer are likely indicative of mixing between surface water and deeper, older water masses. Upwelling is at its maximum during the late spring, and we observe a decrease in DIC $\Delta^{14}\text{C}$ values during this time. Upwelling is stronger further North in the California Current, and transport of these upwelled waters to the SCB may have continued to keep the $\Delta^{14}\text{C}$ values lower during the months after the upwelling maximum (Hickey 1992). The low $\Delta^{14}\text{C}$ values during the winter, when upwelling is weak, could be due to deepening of the mixed layer depth that allows for advection of the deeper, aged water to the surface. The peaks in spring and autumn likely then reflect an increase in the contribution of water from the North Pacific Gyre, which have higher $\Delta^{14}\text{C}$ values (Andrews et al. 2016). This trend overall suggests a steady composition of source waters at our site.

Average seasonal $\delta^{13}\text{C}$ values are strongly seasonal with a minimum during winter and a maximum during summer (Figures 3c and 3d). The seasonality of the two study periods is largely the same, except that, on average, the $\delta^{13}\text{C}$ values were 0.2‰ lower during 2011–2022 than in 2004–2010. The summer maximum suggests that mixing of surface and upwelled water is not the primary control of $\delta^{13}\text{C}$. Deep water DIC typically has lowered $\delta^{13}\text{C}$ due to the remineralization of particulate and dissolved organic matter (Kroopnick 1985). If mixing with upwelled water was the main driver of DIC $\delta^{13}\text{C}$ variability, then we would expect to see decreases in $\delta^{13}\text{C}$ values during the summer months, as we do with $\Delta^{14}\text{C}$ values. Instead, we find a pattern similar to atmospheric $\delta^{13}\text{C}$ CO_2 values. Atmospheric fluctuations in $\delta^{13}\text{C}$ CO_2 values are due to fractionation during terrestrial photosynthesis, which preferentially removes

^{12}C atoms. We hypothesize that the surface DIC $\delta^{13}\text{C}$ at our site fluctuates due to a similar mechanism. As nutrient-rich waters from spring and summer upwelling stimulate primary productivity, the phytoplankton and kelp take up DIC with lower $\delta^{13}\text{C}$ values and thereby increase the $\delta^{13}\text{C}$ of DIC remaining in the water.

The average increase in $\delta^{13}\text{C}$ between March and August is 0.7‰ (Figure 3d). Assuming a concentration of DIC in March of 2.25 mM C (Figure 2c), a DIC $\delta^{13}\text{C}$ of 1.0‰, and a $\delta^{13}\text{C}$ of phytoplankton of -21.0‰, we calculated that 3% (0.07 mM C) of the DIC would need to be fixed by the phytoplankton to produce this increase. Particulate organic carbon concentrations at this site vary seasonally by about 0.03 mM C (Fagan et al. 2019). Assuming a dissolved organic carbon production of a similar magnitude, which is typical in marine settings (Carlson et al. 1998), this suggests that there is sufficient biological fractionation to account for the seasonal variation of DIC $\delta^{13}\text{C}$. This seasonality may be a coastal phenomenon because coasts typically have much higher phytoplankton concentrations than the rest of the ocean (Antione et al. 1996).

4.3 Major Upwelling Event Reflected in DIC $\Delta^{14}\text{C}$ and $\delta^{13}\text{C}$

During the late winter and spring of 2016, we observe an increase in DIC concentration and salinity and decreases in the $\Delta^{14}\text{C}$ and SST (Figures 2a, 2c, 2e, 2f). These features are all consistent with a period of strong upwelling. The CUTI index does show strong fall and winter upwelling during this time period (Figure 2d). This has been attributed to the abrupt end of the 2015–2016 El Niño that resulted in strong upwelling winds (Frischknecht et al. 2017). This unseasonal upwelling created a large positive nutrient anomaly in the region that stimulated higher than normal phytoplankton growth during the winter and early spring. This reduced the amount of nutrients available during the 2016 summer and consequently reduced the phytoplankton abundance during that summer (Frischknecht et al. 2017). During the summer of 2016, the DIC $\delta^{13}\text{C}$ values are lower than other summers (Figure 2b). This is consistent with the hypothesis that primary productivity is the dominant control of $\delta^{13}\text{C}$ in this region.

5. CONCLUSION

This work provides an extended timeseries of surface DIC $\delta^{13}\text{C}$ and $\Delta^{14}\text{C}$ from the Newport Beach Pier for two decades. This series demonstrates the seasonality due to changes in ocean circulation and the continued dilution of these isotopes due to CO_2 from fossil fuel sources. DIC $\delta^{13}\text{C}$ values decreased by 0.03‰ per year with a total decrease of 0.4‰ from 2004 to 2022. DIC $\Delta^{14}\text{C}$ values decreased by 2‰ per year with a total decrease of 42‰ from 2004 to 2022. Between 2004 and 2010, seasonal monthly average $\Delta^{14}\text{C}$ values varied by 11‰ and between 2011 and 2022, monthly average $\Delta^{14}\text{C}$ values varied by 3.4‰. The $\Delta^{14}\text{C}$ variability was likely driven by vertical mixing bringing ^{14}C -depleted waters to the surface and offshore eddies bringing ^{14}C -enriched waters from the gyres to the coastline. Monthly averaged $\delta^{13}\text{C}$ values vary by 0.7‰, likely driven by marine primary productivity, similar to atmospheric CO_2 . The seasonal signal in $\Delta^{14}\text{C}$ is smaller during 2011–2022 than during 2004–2010, but the signal does still correspond to seasonal upwelling, including a major upwelling event in 2016. As $\delta^{13}\text{C}$ and $\Delta^{14}\text{C}$ of both atmospheric CO_2 and surface DIC continue to decline, their relative values may provide vital insight to the rate and magnitude of the fossil fuel CO_2 sink in the ocean, as well as climatic shifts that affect ocean circulation.

SUPPLEMENTARY MATERIAL

To view supplementary material for this article, please visit <https://doi.org/10.1017/RDC.2023.73>

ACKNOWLEDGMENTS

We thank John Southon and all W.M. Keck Carbon Cycle AMS members for their assistance with the ^{14}C and ^{13}C samples. We thank the Newport Beach Lifeguard for the collection of daily temperature and salinity samples as part of the Scripps Shore Stations program. This work was supported by the NSF Chemical Oceanography Program (OCE-1951073) and the Fred Kavli Foundation.

REFERENCES

- Andrews AH, Siciliano D, Potts DC, DeMartini EE, Covarrubias S. 2016. Bomb radiocarbon and the Hawaiian Archipelago: coral, otoliths, and seawater. *Radiocarbon* 58(3):531–548.
- Antoine D, André J, Morel A. 1996. Oceanic primary production: 2. Estimation at global scale from satellite (coastal zone color scanner) chlorophyll. *Global Biogeochemical Cycles* 10(1):57–69.
- Berg N, Hall A. 2015. Increased interannual precipitation extremes over California under climate change. *Journal of Climate* 28(16):6324–6334.
- Bond NA, Cronin MF, Freeland H, Mantua N. 2015. Causes and impacts of the 2014 warm anomaly in the NE Pacific. *Geophysical Research Letters* 42(9):3414–3420.
- Beverly, RK, Beaumont W, Taus D, Ormsby KM, von Reden KF, Santos GM, Southon JR. 2010. The Keck Carbon Cycle AMS laboratory, University of California, Irvine: status report. *Radiocarbon* 52(2):301–309.
- Bray NA, Keyes A, Morawitz WML. 1999. The California current system in the Southern California Bight and the Santa Barbara Channel. *Journal of Geophysical Research: Oceans* 104(C4):7695–7714
- Broecker WS, Peng TH. 1982. Tracers in the sea. Palisades (NY): Lamont-Doherty Geological Observatory, Columbia University. 705 p.
- Bograd SJ, Schroeder ID, Jacox MG. 2019. A water mass history of the Southern California Current System. *Geophysical Research Letters* 46(12):6690–6698.
- Brooks MK. 2020. Time-series of stable isotopes in dissolved inorganic carbon of surface seawater near Bermuda and Hawaii [PhD dissertation]. University of California, San Diego.
- Carlson CA, Ducklow HW, Hansell DA, Smith Jr WO. 1998. Organic carbon partitioning during spring phytoplankton blooms in the Ross Sea polynya and the Sargasso Sea. *Limnology and Oceanography* 43(3):375–386.
- Carter ML, Flick RE, Terrill E, Beckhaus EC, Martin K, Fey CL, Walker PW, Largier JL, McGowan JA. 2022. Shore Stations Program, Newport Beach - Balboa Pier (Newport Beach Archive, 2022-10-24). In: Shore Stations Program Data Archive: Current and Historical Coastal Ocean Temperature and Salinity Measurements from California Stations. UC San Diego Library Digital Collections.
- Dong, C, Idica EY, McWilliams JC. 2009. Circulation and multiple-scale variability in the Southern California Bight. *Progress in Oceanography* 82(3):168–190.
- Druffel ERM, Beauré SR, Ziolkowski LA. 2016. Radiocarbon in the oceans. In: Schuur EAG, Druffel E, Trumbore SE, editors. *Radiocarbon and climate change: mechanisms, applications and laboratory techniques*. Switzerland: Springer International Publishing. p. 139–166.
- Druffel ERM. 1989. Decade time scale variability of ventilation in the North Atlantic: high-precision measurements of bomb radiocarbon in banded corals. *Journal of Geophysical Research: Oceans* 94(C3):3271–3285.
- Fagan AJ, Moreno AR, Martiny AC. 2019. Role of ENSO conditions on particulate organic matter concentrations and elemental ratios in the Southern California Bight. *Frontiers in Marine Science* 6:386
- Feely RA, Sabine CL, Lee K, Berelson W, Kleypas J, Fabry VJ, Millero FJ. 2004. Impact of Anthropogenic CO_2 on the CaCO_3 system in the oceans. *Science* 305(5682):362–366.
- Frankson R, Stevens LE, Kunkel KE, Champion SM, Easterling DR, Sweet W, Anderson M. 2022. California State Climate Summary 2022. NOAA Technical Report. NOAA NESDIS.
- Frischknecht M, Münnich M, Gruber N. 2017. Local atmospheric forcing driving an unexpected California current system response during the 2015–2016 El Niño. *Geophysical Research Letters* 44(1):304–311.
- Gao P, Xu X, Zhou L, Pack MA, Griffin S, Santos GM, Southon JR, Liu K. 2014. Rapid sample preparation of dissolved inorganic carbon in natural waters using a headspace-extraction

- approach for radiocarbon analysis by accelerator mass spectrometry. *Limnology and Oceanography: Methods* 12(4):174–190.
- Gao P, Zhou L, Liu K, Xu X. 2018. Radiocarbon in the maritime air and sea surface water of the South China Sea. *Radiocarbon* 61(2):461–472
- Graven H, Keeling R, Xu X. 2022. Radiocarbon dating: going back in time. *Nature* 607(7919): 449–449.
- Gruber N, Clement C, Carter BR, Feely RA, van Heuven S, Hoppema M, Ishii M, Key RM, Kozyr A, Lauvset SK, et al. 2019. The oceanic sink for anthropogenic CO₂ from 1994 to 2007. *Science* 363(6432):1193–1199.
- Hickey BM. 1992. Circulation over the Santa Monica-San Pedro Basin and Shelf. *Progress in Oceanography* 30(1):37–115.
- Hickey BM. 1979. The California Current System—hypotheses and facts. *Progress in Oceanography* 8(4):191–279.
- Hickey BM, Dobbins EL, Allen SE. 2003. Local and remote forcing of currents and temperature in the central Southern California Bight. *Journal of Geophysical Research: Oceans* 108(C3). <https://doi.org/10.1029/2000JC000313>
- Hinger EN, Santos GM, Druffel ERM, Griffin S. 2010. carbon isotope measurements of surface seawater from a time-series site off Southern California. *Radiocarbon* 52(1):69–89.
- Jacox MG, Edwards CA, Hazen EL, Bograd SJ. 2018. Coastal upwelling revisited: Ekman, Bakun, and improved upwelling indices for the U.S. West Coast. *Journal of Geophysical Research: Oceans* 123:7332–7350.
- Jeansson E, Steinfeldt R, Tanhua T. 2021. Water mass ages based on GLODAPv2 data product (NCEI Accession 0226793). Gv2 PAC age. NOAA National Centers for Environmental Information. Dataset. Accessed May 2023.
- Key RM, Olsen A, van Heuven S, Lauvset SK, Velo A, Lin X, Schirnick C, Kozyr A, Tanhua T, Hoppema M, et al. 2015. Global Ocean Data Analysis Project, Version 2 (GLODAPv2), ORNL/CDIAC-162, NDP-093. Carbon Dioxide Information Analysis Center, Oak Ridge National Laboratory, US Department of Energy, Oak Ridge, Tennessee. Accessed May 2023
- Kroopnick PM. 1985. The distribution of ¹³C of ΣCO₂ in the world oceans. *Deep Sea Research Part A. Oceanographic Research Papers* 32(1):57–84.
- McNaught AD, Wilkinson A. 1997. IUPAC compendium of chemical terminology. 2nd edition. *The Gold Book*. Oxford: Blackwell Scientific Publications.
- Mook WG. 1986. ¹³C in Atmospheric CO₂. *Netherlands Journal of Sea Research* 20(2/3): 211–223.
- Olsen A, Key RM, van Heuven S, Lauvset SK, Velo A, Lin X, Schirnick C, Kozyr A, Tanhua T, Hoppema M, et al. 2016. The Global Ocean Data Analysis Project version 2 (GLODAPv2) – an internally consistent data product for the world ocean. *Earth System Science Data* 8:297–323.
- Quay P, Sonnerup R, Munro D, Sweeney C. 2017. Anthropogenic CO₂ accumulation and uptake rates in the Pacific Ocean based on changes in the ¹³C/¹²C of dissolved inorganic carbon. *Global Biogeochemical Cycles* 31(1):59–80.
- Sabine CL, Feely RA, Gruber N, Key RM, Lee K, Bullister JL, Wanninkhof R, Wong CS, Wallace DWR, Tilbrook B, et al. 2004. The oceanic sink for anthropogenic CO₂. *Science* 305(5682): 367–371.
- Santos, G M, Ferguson J, Acaylar K, Johnson KR, Griffin S, Druffel ERM. 2011. D¹⁴C and D¹³C of seawater DIC as tracers of coastal upwelling. *Radiocarbon* 53(4):6690677.
- Seager RI, Hoerling M, Schubert S, Wang H, Lyon B, Kumar A, Nakamura J, Henderson N. 2015. Causes of the 2011–14 California drought. *Journal of Climate* 28(18):6997–7024.
- Stuiver M, Polach HA. 1977. Discussion: reporting of ¹⁴C data. *Radiocarbon* 19(3):355–363.
- Stuiver M, Pearson GW, Braziunas T. 1986. Radiocarbon age calibration of marine samples back to 9000 cal yr BP. *Radiocarbon* 28(2B): 980–1021.
- Suess HE. 1953. Natural radiocarbon and the rate of exchange of carbon dioxide between the atmosphere and the sea. In: Aldrich LT, editor. *Proceedings of Conference on Nuclear Processes in Geological Settings*. National Research Council, Commission on Nuclear Science 1:52–56.
- Torres, ME, Mix AC, Rugh WD. 2005. Precise Δ¹³C analysis of dissolved inorganic carbon in natural waters using automated headspace sampling and continuous-flow mass spectrometry. *Limnology and Oceanography: Methods* 3(8):349–360.
- Virtanen P, Gommers R, Oliphant TE, Haberland M, Reddy T, Cournapeau D, Burovski E, Peterson P, Weckesser W, Bright J, et al. 2020. SciPy 1.0 Contributors. *SciPy 1.0: Fundamental Algorithms for Scientific Computing in Python*. *Nature Methods* 17(3):261–272.
- Weber ED, Auth TD, Baumann-Pickering S, Baumgartner TR, Bjorkstedt EP, Bograd SJ, Burke BJ, Cadena-Ramírez JL, Daly EA, de la Cruz M, et al. 2021. State of the California Current 2019–2020: back to the future with marine heatwaves? *Frontiers in Marine Science* 8:709454.
- Xu X, Trumbore SE, Zheng S, Southon JR, McDuffee KE, Luttgren M, Liu JC. 2007. Modifying a sealed tube zinc reduction method for preparation of AMS graphite targets: reducing background and attaining high precision. *Nuclear Instruments and Methods in Physics Research B* 259(1):320–329.

APPENDIX

Table 1 $\Delta^{14}\text{C}$ values, $\delta^{13}\text{C}$ values, and concentrations of surface DIC samples.

Date collected	UCI AMS#	$\Delta^{14}\text{C}$ (‰)	\pm^1	$\delta^{13}\text{C}$ (‰) ²	Concentration (mM C) ³
1/10/11	136164	8.3	2.3		
1/10/11	136161	10.6	2.5	0.67	2.34
2/13/11	99410	15.5	1.9		
2/13/11	99411	19.6	1.9		
4/12/11	129994	17.5	2.6		
4/12/11	129995	14.4	2.6		
5/12/11	99412	17.1	1.8		
5/12/11	99413	15.8	2.0		
6/13/11	99414	15.1	1.8		
6/13/11	99415	16.0	2.1		
7/13/11	99416	15.9	1.8		
7/13/11	99417	16.9	1.8		
8/11/11	99418	16.5	1.9		
8/11/11	99419	16.5	2.2		
9/13/11	136165	15.9	2.5		
9/13/11	99420	13.7	1.9	1.49	2.22
9/13/11	99421	16.3	2.0		
10/15/11	133972	10.1	1.9		
11/15/11	128696	11.8	1.9	1.41	2.21
11/15/11	128697	11.6	1.9		
11/15/11	128698	10.5	1.8		
11/15/11	128699	7.2	2.0		
11/15/11	136158	14.3	2.4		
12/14/11	129997	15.3	2.6		
12/14/11	129998	15.3	2.6		
12/14/11	129999	16.4	2.9		
1/12/12	130003	15.3	2.6		
1/12/12	130004	11.4	2.6		
1/12/12	130005	14.3	2.6		
1/12/12	130006	17.4	2.7		
3/15/12	136160	22.1	2.6		
4/12/12	129996	20.9	2.6		
4/12/12	130001	12.6	2.7	0.49	2.35
5/17/12	136166	15.4	2.4	1.04	2.35
6/14/12	136159	16.7	2.4	1.49	2.26
7/23/12	136167	16.8	2.4	1.63	2.22
8/17/12	136168	15.5	2.4	1.44	2.23
8/17/12				1.51	2.27
9/19/12	136169	17.7	2.6	1.62	2.29
11/14/12	136167	18.8	2.4	1.06	2.28
1/10/13	136643	12.6	3.3	1.22	2.29
2/7/13	136654	16.0	2.7		

(Continued)

Table 1 (Continued)

Date collected	UCI AMS#	$\Delta^{14}\text{C}$ (‰)	\pm^1	$\delta^{13}\text{C}$ (‰) ²	Concentration (mM C) ³
2/7/13	136655	9.5	2.7		
3/12/13	136151	19.4	2.4	0.91	2.28
4/18/13	136152	9.2	2.7		
4/18/13	136161	10.6	2.5	0.67	2.34
5/9/13	136153	17.1	2.8	1.37	2.26
6/6/13	136644	13.0	2.7		
7/6/13	136645	14.8	2.7		
7/6/13	136646	14.2	2.7		
8/2/13	136647	4.4	3.0	1.28	2.68
8/27/13	136648	15.5	2.7	1.61	2.26
10/9/13	136649	22.0	2.7	1.71	2.21
11/4/13	136650	14.7	2.7		
12/4/13	136651	12.3	2.7	1.14	2.26
1/9/14	136652	11.1	2.7		
1/9/14	136656	9.2	2.7		
2/10/14	164582	12.2	2.9	1.18	2.27
3/13/14	164583	12.4	2.7	1.47	2.22
4/7/14	164584	12.2	2.6	2.14	2.17
5/8/14	164585	10.3	2.5	1.19	2.28
6/3/14	164586	12.4	2.6	1.40	2.25
7/7/14	164587	10.3	2.6	1.73	2.24
8/4/14	164588	9.2	2.8	1.50	2.26
9/16/14	164589	7.6	2.6	1.53	2.26
10/7/14	164590	10.1	2.7	1.50	2.24
11/25/14	164591	10.1	2.6	1.39	2.24
1/9/15	164592	9.2	2.6	1.32	2.26
2/6/15	164593	10.3	2.7	1.14	2.24
3/23/15	164594	10.1	2.8		
4/29/15	164595	10.2	2.8	1.38	2.22
5/27/15	164596	5.2	2.6	1.33	2.33
5/27/15				1.26	2.3
6/17/15	164597	10.0	2.7	1.44	2.24
7/24/15	191748	5.2	1.5	1.38	2.26
8/28/15	191743	5.2	1.5	1.63	2.29
9/22/15	191749	8.6	1.6	1.41	2.22
10/30/15	191744	6.7	1.6	-0.30	2.32
11/30/15	191745	11.1	1.6	1.45	2.23
12/18/15	191746	5.6	2.0	1.33	2.30
1/29/16	191747	7.1	1.5		
1/29/16	262143	3.2	1.6	1.05	2.39
3/28/16	171954	2.3	1.6		
3/28/16	227518	-2.9	2.6	1.15	2.39
3/28/16	229231	-3.9	2.4		
3/28/16	262144	3.2	1.6	1.11	2.37
4/29/16	191755	4.7	1.6		

Table 1 (Continued)

Date collected	UCI AMS#	$\Delta^{14}\text{C}$ (‰)	\pm^1	$\delta^{13}\text{C}$ (‰) ²	Concentration (mM C) ³
4/29/16	262145	4.5	1.9	1.21	2.38
5/27/16	191758	-1.1	1.4		
5/27/16	265836	5.3	1.9	1.34	1.99
6/24/16	191759	1.8	1.4	1.15	2.29
7/28/16	191763	-4.1	1.6		
9/1/16	191764	-1.4	1.6	1.25	2.23
4/20/17	262147	9.5	1.6	1.33	2.34
4/20/17	262148	12.7	1.7	1.30	2.33
6/1/17	262151	1.7	1.6	1.44	2.35
6/1/17	262152	2.7	1.6		
7/18/17	262153	6.3	1.8	2.12	2.27
8/23/17	262154	6.6	1.7	1.56	2.34
10/31/17	262155	3.1	1.6	1.43	2.33
12/5/17	262156	7.8	1.6	1.02	2.35
10/18/18	262158	8.6	1.6	1.14	2.29
11/21/18	227508	7.2	2.7	1.08	2.26
11/21/18				1.11	2.24
12/20/18	262158	4.0	1.6	0.87	2.33
12/20/18	265837	7.6	1.7		
1/24/19	262160	8.0	1.8		
1/24/19	262161	2.2	1.6	0.98	2.32
3/19/19	262163	3.9	2.3	1.14	2.30
4/18/19	262164	3.0	2.2	1.09	2.29
6/26/19	262166	2.5	1.8	1.03	2.31
8/28/19	229270	4.0	2.3		
8/28/19	227505	5.4	2.6		
8/28/19	227506	8.8	2.6		
8/28/19	227509	5.3	2.8		
8/28/19	262169	-4.6	1.8	2.09	2.23
9/29/19	262170	5.7	1.8		
9/29/19	262584	7.0	2.3	1.43	2.28
10/29/19	227510	5.3	2.6		
11/19/19	229233	6.2	2.3		
11/19/19	229234	1.6	2.2		
11/19/19	262171	1.5	1.9	1.10	2.25
1/20/20	262172	-2.7	2.0	0.93	2.42
2/27/20	262173	2.4	1.9	0.93	2.30
6/16/20	262174	2.0	1.7	1.34	2.59
6/16/20	262175	3.3	1.7	1.50	2.27
7/30/20	262176	-5.5	1.7	1.10	2.62
8/24/20	262177	-7.2	1.8	1.80	2.25
9/18/20	262178	-8.0	2.0	1.72	2.31
9/18/20	162585	-2.6	1.6	1.66	2.26
10/20/20	262179	1.6	1.7	1.52	2.04
3/11/21	262180	-6.3	2.1	0.61	2.67

(Continued)

Table 1 (Continued)

Date collected	UCI AMS#	$\Delta^{14}\text{C}$ (‰)	\pm^1	$\delta^{13}\text{C}$ (‰) ²	Concentration (mM C) ³
3/11/21	265842	-0.3	1.8		
3/11/21	265843	-2.0	1.8		
4/20/21	262181	-2.3	1.7	1.05	2.29
4/20/21	262182	1.2	2.3	1.04	2.36
5/14/21	262183	-0.3	2.2	1.08	2.67
6/25/21	262184	-5.3	1.7	1.39	2.26
8/17/21	262185	-5.4	1.7	1.61	2.22
9/30/21	262186	-7.1	1.4	1.34	2.26
9/30/21				1.40	2.26
9/30/21	262586	-4.7	1.6		
10/7/21	262187	-5.6	1.6	1.39	2.24
10/15/21	262188	-5.8	1.6	1.12	2.25
10/28/21	262189	-4.7	1.7	1.69	2.17
12/21/21	262190	-12.6	1.7	1.07	2.26
12/21/21	265844	-4.0	1.8		
1/19/22	262587	-4.8	1.6	1.23	2.23
2/18/22	262588	-4.8	1.6	1.17	2.23
3/17/22	262191	-5.7	1.5	0.89	2.25
4/13/22	262141	-8.4	1.9	1.19	2.24
4/13/22	262582	-3.0	1.8	1.04	2.30
5/16/22	265845	-4.7	1.7	1.24	2.19

¹Listed values represent AMS error. Pooled standard deviation of replicates is 2.6‰.

²Pooled standard deviation of replicates is 0.1‰.

³Pooled standard deviation of replicates is 0.01 mM C.